Available online at www.sciencedirect.com
SCIENCE DIRECT®
International Journal of Heat and Fluid Flow 25 (2004) 1–9
International Journal of HEAT AND FLUID FLOW
www.elsevier.com/locate/ijhff

Vortices behind a bluff body with an upswept aft section in ground effect

X. Zhang *, A. Senior, A. Ruhrmann

Aerospace Engineering, School of Engineering Sciences, University of Southampton, Southampton SO17 1BJ, UK

Received 24 March 2003; accepted 11 November 2003

Abstract

The vortices behind a bluff body equipped with an upswept aft section are studied in a model test. The bluff body operates in close proximity to ground. The principle measurement technique is laser Doppler anemometry (LDA), which is supported by surface flow, pressure and force measurements. The upswept surface has an angle of 17° to horizontal. With the presence of end-plates on the aft section, discontinuities in slope of the force curve exist at several heights in proximity to the ground. The characteristics of these changes are linked with edge vortices. The position and strength of the vortex are identified. Three main types of trailing vortices exist: (a) concentrated, symmetric with a high axial speed core, (b) diffused, symmetric with a low axial speed core, and (c) diffused and asymmetric. The study provides further clarification of major physics and a database for validating predictive methods.

Keywords: Bluff body; Diffuser; Ground effect; Vortex flow

1. Introduction

Large vortices generated by aerodynamic surfaces near a ground plane are of both fundamental and practical interests. They can be employed as a means for flow control. There are various types of *vortex in ground effect*. Of particular interest to the present authors are the large vortices associated with a bluff body operating in proximity to a ground plane, where the sizes of the vortices are in the same order as that of the model geometry. Often a deceptively simple configuration would lead to complex force behaviours and to trailing vortices embedded in a highly turbulent wake. In engineering applications, a bluff body operating in close proximity to a ground plane has its applications in the automobile industry (Bearman, 1980). A carefully planned study can provide a validating case for predictive methods such as those employing large eddy simulation.

In this study, we focus on a bluff body equipped with an upswept aft section. When placed in ground effect, an effective expansion/diffuser section is formed between the upswept surface and the ground. This configuration has been utilized primarily on high performance vehicles to increase downforce, i.e. negative lift, therefore enhancing the overall mechanical grip. An important feature of the flow is that the pressure at the base of the bluff body remains relatively constant as the model height is varied (Senior and Zhang, 2001). Hence as the model height is reduced, pressure underneath of model (nearest to the ground plane) must be 'pumped down' (Sovran, 1994), which leads to an increase in downforce. The downforce works in conjunction with the mechanical grip, to improve the performance of the vehicle. However, it is not only the overall level of downforce that is the important factor. The upswept surface changes height from the ground, due to the suspension movements on the vehicle. This severely affects the level of downforce, hence the grip at the rear and the force balance. There is also a safety consideration as the wake generated by the bluff body will have an impact on the aerodynamic (and handling) performance of a trailing vehicle.

There have been a number of relevant studies (George, 1981; George and Donis, 1983; Cooper et al., 1998, 2000), looking at the forces, surface pressures and surface flow

* Corresponding author. Tel.: +44-23-8059-4891; fax: +44-23-8059-3058.
E-mail address: xzhang@soton.ac.uk (X. Zhang).

0142-727X/$ - see front matter © 2003 Elsevier Inc. All rights reserved.
doi:10.1016/j.ijheatfluidflow.2003.11.002

Nomenclature

A	frontal area of the model
C_L	downforce coefficient, positive downwards; $L/(q_\infty A)$
C_D	drag coefficient; $D/(q_\infty A)$
c_p	pressure coefficient; p/q_∞
D	drag
d	half-width of model; 157 mm
h_r	height of model above moving ground
L	negative force or downforce
p	pressure
q_∞	dynamic head
U_∞	freestream velocity
u, v, w	mean velocities in x, y, z directions
$\overline{u'u'}, \overline{v'v'}, \overline{w'w'}$	normal Reynolds stresses in x, y, z directions
x, y, z	cartesian coordinates: x+ve downstream, y+ve up, z+ve to port

Greeks

Ω	streamwise vorticity
$\delta_{0.99}$	boundary layer thickness
ξ, η, ζ	local coordinates: ξ+ve downstream, η+ve normal, ζ+ve tangential to port
ρ	density

Subscript

∞	freestream

generated by bluff body/diffusers in ground effect. However, a number of major issues still remain unresolved. These include the precise mechanics of force behaviours, e.g. the loss of downforce, the role of trailing vortices, and the effect of the ground. It seems that it is vitally important to model the ground correctly. Using a *fixed ground* will not give correct physics and would produce results no better than freestream tests. It is also important to conduct off-surface studies rather than relying solely on on-surface flow visualisation and pressure measurements, as large vortices play an important role in defining the overall behaviours. Apart from engineering and fundamental interests, correctly conducted tests and off-surface measurements, including turbulence data, would benefit numerical modelling efforts.

In a recent study (Senior and Zhang, 2001), the overall force and on-surface features of a bluff body equipped with an aft upswept section were investigated in ground effect in wind tunnel model tests that employs a moving ground. As the bluff body is lowered towards the ground from a height in freestream, the overall downforce on the body first experiences an increase, the *force enhancement* phenomenon. The enhancement process can be divided into two stages: a rapid rising stage and a slow varying stage, before the appearance of the *force reduction* phenomenon when the model is lowered below a critical height. This observation is important in engineering applications such as a racing car. To maintain the balance of a car, rapid changes in downforce should be avoided. Hence a slow varying downforce curve over a range of heights should be an advantage. It has been speculated that the abrupt changes in the gradient of the downforce curve are due to changes in the vortex characteristics. However, with only on-surface measurements, it is difficult to shed much light on the precise physics. It is felt that a major ingredient, some would say the most important part, of the overall flow physics is the large vortices generated off the aft section. Off-surface measurements, such as laser Doppler anemometry (LDA), particle image velocimetry (PIV), hot wire anemometry (HWA), and pressure probes, would provide further insight into the phenomenon. In the study reported here, LDA is employed as the main technique to clarify major physics and to identify possible links between off-surface features and force behaviour.

2. Description of experiments

2.1. Bluff body model and test facilities

The generic model incorporates main features of the aft diffuser section of a high performance vehicle. These are an upswept surface with side-plates, a flat-bottomed surface upstream of the aft section to replicate the undertray of the vehicle, a bluff base and a means of preventing flow separation at the leading edge of the model so that air is permitted a clear pathway to the diffuser section.

The model consists of a front round nose, a mid-section and an aft section with an underside upswept surface of 17°. The upswept surface is closed on both sides by thin side plates. The model is symmetric about the span-wise central plane. Detailed dimensions of the model can be found in Senior and Zhang (2001) and are also provided in Fig. 1. The model is mounted on a strut connected to an overhead force balance. The boundary layer on the model surface is tripped by a 0.4 mm diameter piano wire at $x/d = 0.637$ behind the nose. The location of transition is fixed to avoid a laminar separation bubble developing over the nose top surface, and also so that computational simulations could be designed to transition at a fixed location.

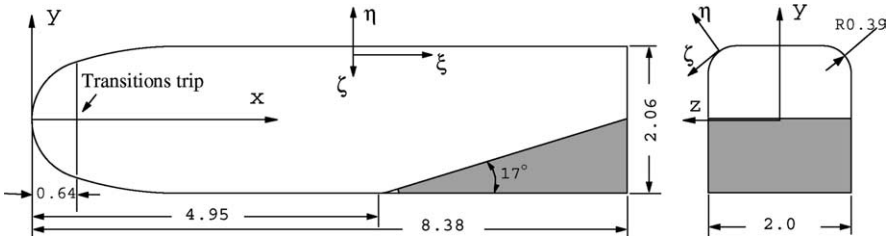

Fig. 1. A schematic of the test model. All dimensions normalised by half-width d. Shadow area indicates the end-plates and the ramp surface.

The Southampton 3.5 m×2.5 m and 2.1 m×1.5 m tunnels are used in the study, with the larger tunnel for LDA tests and the smaller one for others. In the 2.1 m×1.5 m the blockage caused by the model is 2.86% and in the 3.5 m×2.5 m—1.12%. The closed circuit tunnels are equipped with a moving ground to correctly simulate road conditions. Turbulence levels are less than 0.2%. Reynolds number is around 5.4×10^6 based on the width of the model and a wind tunnel speed of 20 m/s.

2.2. Measurements

Non-intrusive flow field measurements are undertaken using a 3-component LDA system, with a 5 W Arion laser (for details see Zhang, 1998). Seeding particles 3 μm in diameter are used. Approximately 1000 samples are collected at each data point. Other tests conducted include force balance, surface pressure taps, and oil flow visualisation.

Applying the SSU procedure described by Moffat (1988) the single sample uncertainties in the experiment are calculated. The model height is kept to within ±0.1 mm and the yaw angle is set to ±0.05°. At a typical height, the uncertainties in the C_L and C_D measurements are ±0.0056 and ±0.0008 respectively. The uncertainty in the pressure measurements for a c_p of −2.0 is ±0.0188.

The uncertainties and 95% confidence interval in the LDA data are estimated using procedures given by Moffat (1988) and Benedict and Gould (1996) respectively. The uncertainties in the mean velocity measurements are ±0.09, ±0.09 and ±0.31 m/s for u, v, w, where u, v, w are defined in the x, y, z directions respectively. Typical 95% uncertainties in the normal stress measurements are less than 8%.

3. Results and discussion

Unless otherwise stated, most of the LDA results presented here are measured at a distance of 15 mm downstream of the model ($x/d = 8.476$). Measurements (including turbulence stress measurements) are also conducted at $x/d = 9.43$ and 10.39 but the results are not included.

3.1. Flow at $h_r/d = 4.14$

In an attempt to define the behaviour of the flow away from the ground plane, measurements were taken at a height of $h_r/d = 4.14$, where the model is positioned roughly at the centre of the working section. At this height, the effect of the ground plane is small (Senior and Zhang, 2001). Surveys are made of boundary layer above and beneath the model along the centreline (not shown) and on the cross-plane at the inlet to the aft ramp (Fig. 2). Above the model (not shown), $\delta_{0.99}$ increases from 7 mm at $x/d = 2.3$ to 15 mm at $x/d = 5.5$. Underneath the model the flow accelerates along the flat bottom. $\delta_{0.99}$ increases from 11.9 mm at $x/d = 3.0$ to 15.4 mm at $x/d = 4.5$. The profile measured at $x/d = 4.9$ is immediately upstream of the ramp inlet, and shows a large flow acceleration, reaching a speed of $u/U_\infty = 1.374$.

Measurements taking at $x/d = 4.95$ (Fig. 2) point to a highly three-dimensional inlet flow. The actual area of the measurements covers the whole of the inlet span. However, the flow is symmetric about the model centreline at this height; therefore only half of the span is presented here. At the inlet, the local low pressure leads to strong entrainment either side of the model. The streamwise velocity remains highest under the model centreline. However the cross-flow velocities are higher underneath the model sides.

The flow immediately behind the diffuser exit, at $x/d = 8.476$, is shown in Fig. 3. A highly concentrated vortex is formed just off the edge of the side plate. The vortex possesses a high axial speed core (e.g. Menke and Gursul, 1997). The highest streamwise velocity is measured at $u/U_\infty = 1.07$. Results at the centre of the vortex at this height could not be obtained due to an absence of seeding. It is surmised that the seeding moves towards the outside of the core along the length of the vortex due to the centripetal forces acting on the particles. The phenomenon was also reported by Payne et al. (1988) in their smoke flow visualisation of vortices over a delta wing, and by Yeung and Lee (1999) in their PIV study of a wing tip vortex. The flow surrounding the core is high speed in the streamwise and cross-flow directions; the maximum cross-flow velocities are $v/U_\infty = 0.67$ and $w/U_\infty = 0.86$ on the measurement plane; vorticity levels

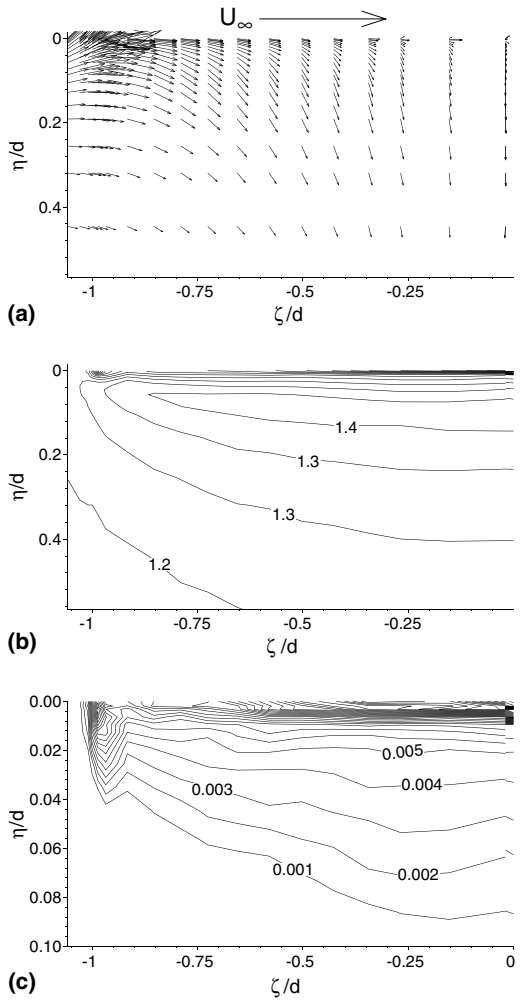

Fig. 2. Cross-plane flow at the inlet of the ramp at $x/d = 4.95$: (a) cross-plane velocity vectors, (b) u/U_∞ contours, (c) $\overline{u'u'}/U_\infty^2$ contours. Origin of the local coordinate system is located at $x/d = 8.38$, $y/d = 0$, $z/d = 0$.

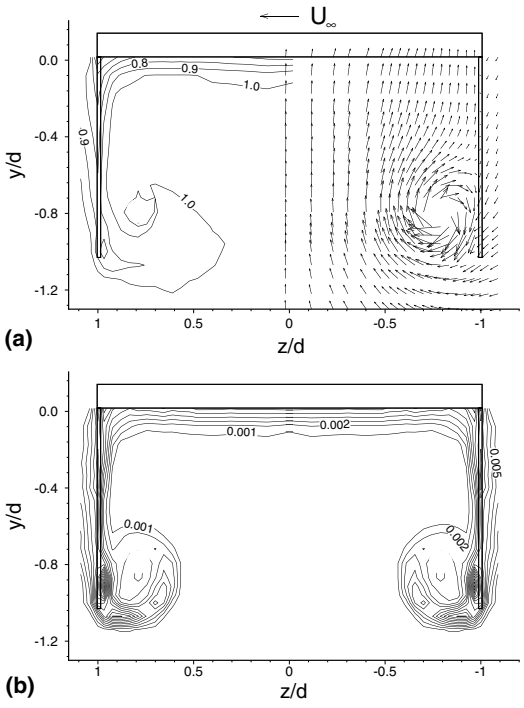

Fig. 3. Concentrated vortices behind the diffuser at $h_r/d = 4.14$; $x/d = 8.476$: (a) u/U_∞ contours and cross-plane velocity vectors, (b) $\overline{u'u'}/U_\infty^2$ contours.

at the centre are also high. The shear layer formed off the upswept surface by the separated boundary layer is visible in both the streamwise velocity contours and the stress contours as well. A large area of the exit flow is occupied by a nearly uniform flow of $u/U_\infty = 1.018$, slightly above the freestream value. Flow is entrained underneath the side-plates and is wound into the vortices, the directions of the induced flows of the two vortices being diametrically opposite to each other. The flow between them forms an upwash. The flow at the diffuser ramp remains attached across the span of the model, and in the corner regions of the diffuser the boundary layer appears to be thicker. This distribution is typical of rectangular channel flows (Brundrett and Baines, 1964). The normal stress distribution suggests a nearly uniform distribution across the ramp surface, as expected of an attached ramp flow, and also indicates that the low turbulence level of the flow exiting the diffuser, excepting the shear layer rolling up into the vortex.

3.2. A review of force behaviour

The force curve can be divided into four main regions (Fig. 4): force enhancement (a), force plateau (b), force reduction (c) and loss of downforce (d), broadly following Senior and Zhang (2001). However unlike Senior and Zhang (2001), hysteresis in the forces are observed between the force reduction region and the force plateau region, which is marked by symbol b/c in Fig. 4.

With the presence of the upswept section, the flow is accelerated more over the underside of the model than over the upper side. This creates a negative lift directed towards the ground, i.e. downforce. The effect of the ground is to constrain the flow beneath the model. Therefore when the model is placed in ground effect, the flow is accelerated more over the ramp surface than for the case out of ground effect in freestream. This causes a peak suction at the entry to the upswept section and a greater pressure recovery demand (Senior and Zhang, 2001). The result is an increase in the total downforce on the model comparing with that in freestream. When the ground height is reduced, this effect becomes more pronounced; the peak suction increases at the inlet to the ramp. We note that the downforce in region (a) does not follow a linear behaviour but experiences an exponential rise with a reduction in model height. It is sur-

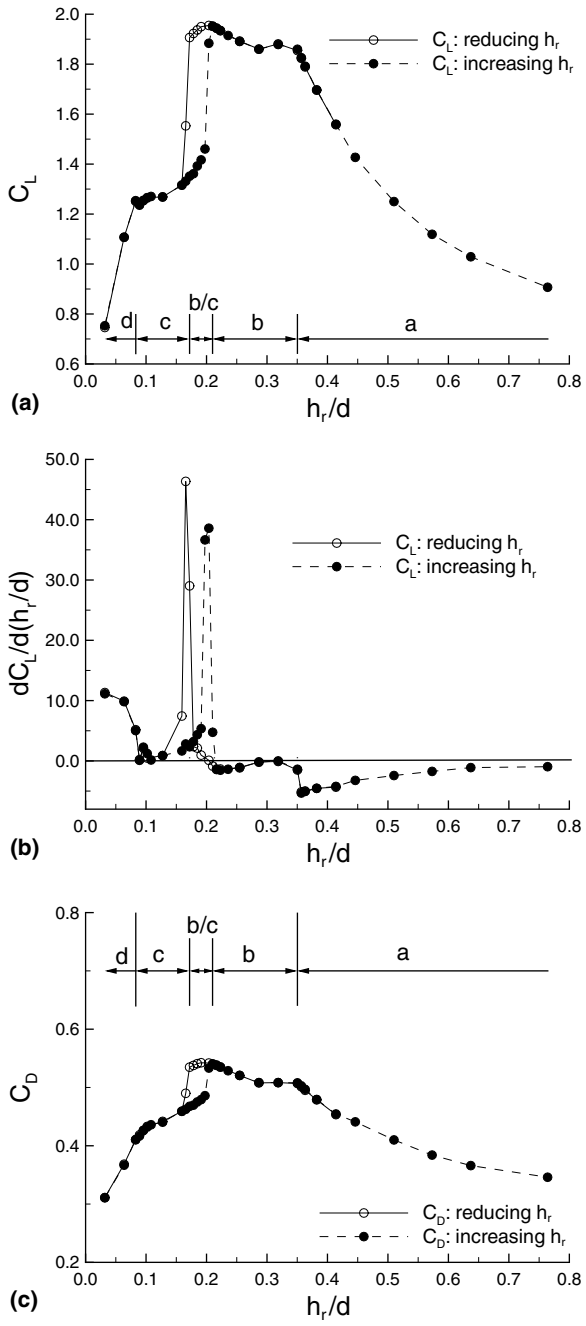

Fig. 4. Downforce vs model height curve: (a) force, (b) slope, (c) drag.

mised that the additional contribution is supplied by the strong edge vortex (see Fig. 3). At a critical height where the pressure recovery is sufficiently steep, separation occurs at the ramp surface. For the present flow, this occurs at $h_r/d = 0.350$. At this height, the slope of the force curve experiences a sudden change (Fig. 4(b)). As the height is reduced further, the downforce will first drop and then increases linearly (region (b)). The downforce reaches a maximum, due to large scale separation on the ramp surface. Below the maximum downforce height, there is a sudden reduction in downforce, which is commonly referred to as the downforce reduction phenomenon. About a third of total downforce could be lost. As the model height is reduced below the maximum downforce height, the downforce would follow a steady decline curve towards the ground (region (c)). In between the regions (b) and (c), hysteresis exists between $h_r/d = 0.172$ and 0.210. A further reduction in the model height leads to a total loss of downforce gain (region (d)).

3.3. Contra-rotating edge vortices

The nonlinear force behaviour reported above and the difference in the downforce behaviour at the junction of regions (a) and (b) suggest changes in the major physics. The base pressure of the bluff body is governed by the flow separation at edge of the bluff base; it experiences little variation with the model height in regions (a) and (b) (Senior and Zhang, 2001). As the model height is reduced, the accelerated flow underneath the model ensures an increased level of suction, leading to downforce enhancement (Sovran, 1994). However, differences in regions (a) and (b) point to the existence of additional factors in the force enhancement process, such as the presence of force enhancement vortices, which warrants a further study.

The existence of the edge vortex is clearly shown in Fig. 3. The pressure difference across the side plate leads to flow entrainment across the edge of the side plate. The flow separates at the edge forming a shear layer. The rolling up of the shear layer forms an attached vortex inside the upswept section which then trails downstream.

As the model height is lowered into region (a), the basic features of the flow remain the same as those at $h_r/d = 4.14$ (Figs. 5(c) and 6(c)). The boundary layer is seen to stay mainly attached to the surface of the ramp, as is evident in Fig. 6(c). Due to the constraining effect of the ground, the streamwise velocity underneath the model is higher than that at $h_r/d = 4.14$. The maximum cross-flow velocities are $|v/U_\infty| = 1.34$ and $|w/U_\infty| = 1.40$. The main vortex now moves further inboard and its size becomes progressively larger as the model height is reduced in region (a).

Also in this region, the high axial speed core of the edge vortex remains, and its speed at $h_r/d = 0.382$ was estimated at $u/U_\infty = 1.59$, though the actual value may be higher. There does not exist a strong induced shear flow off the ground in this flow region. We can, however, detect regions of induced cross-flow separation on the ground in the stress results (not included). The effect of the vortices can be seen in Fig. 7(a) where the surface streaklines are shown. The flow on the upswept surface stays attached and is symmetrical. There exists an induced, secondary vortex flow at the junction between the upswept surface and the side plate. From the surface

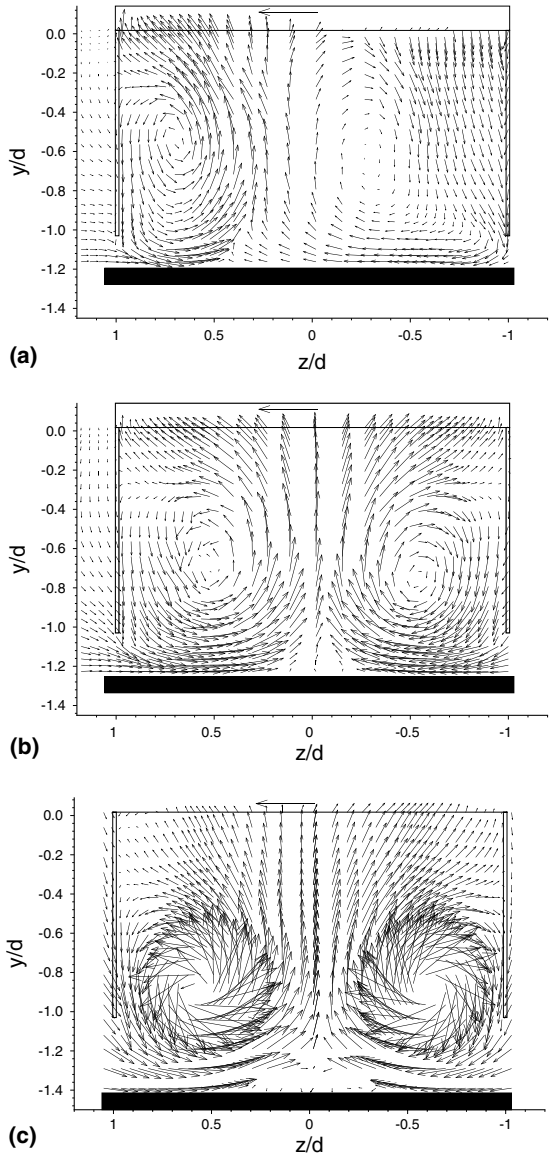

Fig. 5. Mean velocity vectors at $x/d = 8.476$: (a) $h_r/d = 0.159$, (b) $h_r/d = 0.217$, (c) $h_r/d = 0.382$. Unity reference vector.

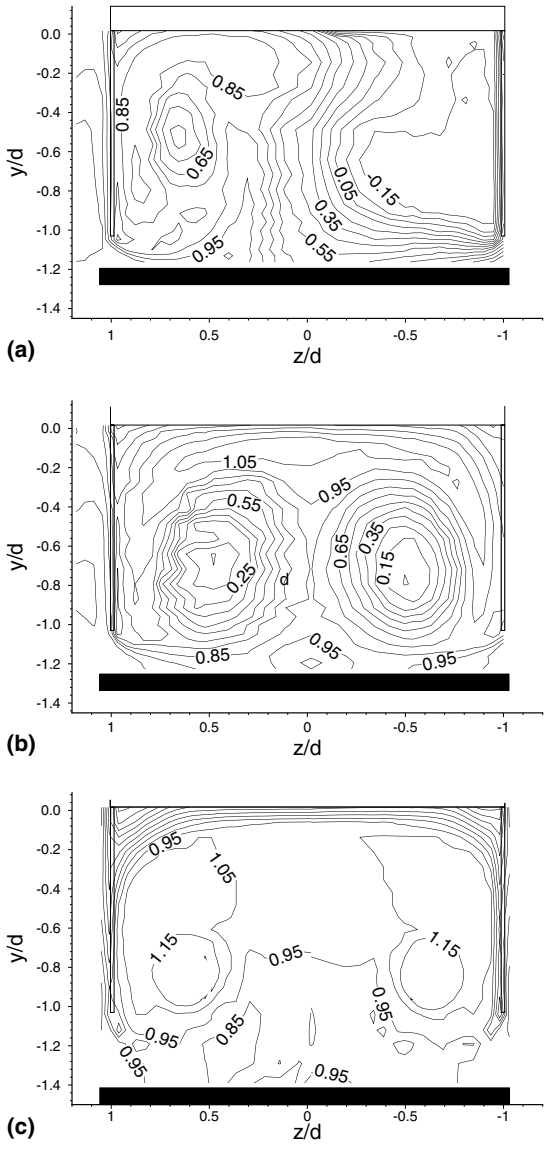

Fig. 6. u/U_∞ contours at $x/d = 8.476$: (a) $h_r/d = 0.159$, (b) $h_r/d = 0.217$, (c) $h_r/d = 0.382$.

streaklines, it can be seen that the main vortex initiates from the leading corner of the upswept section, at the junction of the side plate and the upswept surface. It then grows along the side plate. There is vortex induced suction on both the upswept surface and the inside of the side plate. The exponential component in the downforce can be attributed to the vortex induced suction. Indeed the drag follows the same trend as the downforce (Fig. 4(c)), suggesting an induced drag (vortex drag) contribution (Jones, 1990). The highly concentrated vortex core suggests a stable vortex flow.

There are clear differences between the vortices in regions (a) and (b), in terms of size, core characteristics, strength and distribution. When the model height is moved into region (b), an abrupt change in the flow characteristics occurs. The surface flow pattern is rather similar to that observed by Morel (1978) for base-slant flows. In order to explain the difference in the downforce of low angle diffuser and high angle diffuser flows, Cooper et al. (1998) had suggested that the surface flow separation is the main factor. Indeed separation is observed on the upswept surface (Fig. 7(b)). However, Senior and Zhang (2001) had observed a continuous rise in the peak suction level over this flow region as the model height is reduced. It suggests that a major factor in the force enhancement process is still present. In fact, the downforce and drag vs. height curves resume an almost linear behaviour after the initial 'plateau' at the beginning of the region (b) (Fig. 4(a)). Oil flow observation also indicates the limited extent of the separation

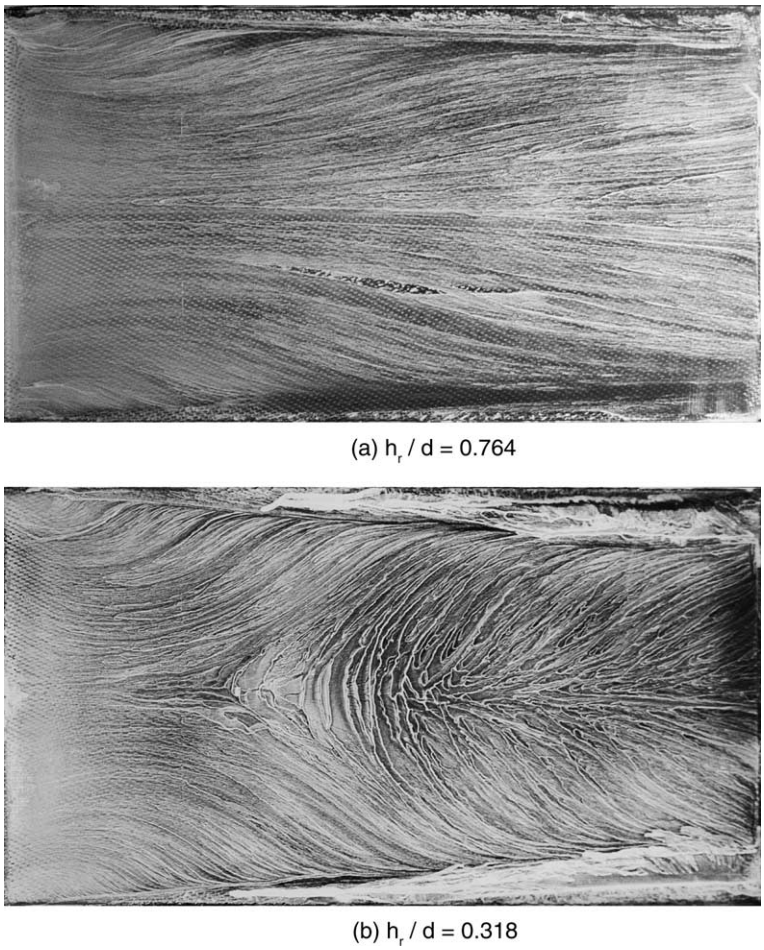

Fig. 7. Oil flow visualisation of surface streaklines on the upswept surface. Flow from left to right.

(Fig. 7(b)). What is revealing is the sudden increase in the size of the vortex after the separation.

In Figs. 5(b) and 6(b), changes in the vortex characteristics are shown in region (b). The mean velocity field remains broadly symmetric, though there are differences in the size of the vortices. The size of the vortex is increased substantially, compared to that in region (a). A low axial speed core now exists at the centre of the vortex (see Table 1). At $h_r/d = 0.318$ (not shown), the axial speed at the centre of the right side vortex is $u/U_\infty = 0.229$ which reduces to 0.081 at $h_r/d = 0.217$. The strength of the vortex has also experienced a sharp reduction. Peak vorticity level ($\Omega d/U_\infty$) is now −10.23 at $h_r/d = 0.318$, reducing further to −3.76 at $h_r/d = 0.217$. In region (a), a typical value would be in the order of O(40) at $h_r/d = 0.382$. The maximum cross-flow velocities are $|v/U_\infty| = 0.89$ and $|w/U_\infty| = 0.86$ at $h_r/d = 0.318$, and 0.59 and 0.66 at $h_r/d = 0.217$ respectively. A low axial speed core and vortex dilation are features of vortex breakdown (Lambourne and Bryer, 1962; Delery, 1994). The drag vs. height curve shown in Fig. 4(c) follows closely the downforce curve, suggesting the loss

Table 1
LDA cross-plane vortex flow at $x/d = 8.476$

h_r/d	u_c/U_∞		$\mathrm{TKE}_c/U_\infty^2$		y_c/d		z_c/d		$\Omega_c d/U_\infty$	
	ls	rs	ls	rs	ls	rs	ls	rs	ls	rs
0.064	−0.058	n/a	0.027	n/a	−0.797	n/a	n/a	−0.529	n/a	−0.23
0.159	−0.161	0.459	0.050	0.073	−0.632	−0.541	0.690	−0.285	4.97	−1.08
0.204	0.186	−0.261	0.084	0.035	−0.688	−0.746	0.490	−0.584	1.15	−8.10
0.217	0.064	0.081	0.092	0.074	−0.750	−0.692	0.532	−0.540	3.25	−3.76
0.255	0.036	0.029	0.077	0.081	−0.752	−0.727	0.493	−0.510	5.02	−3.67
0.318	0.096	0.229	0.062	0.050	−0.801	−0.820	0.545	−0.557	7.36	−10.23

of the induced drag (vortex drag) as described by Munk (Jones, 1990).

Measurements of streamwise velocity reveal that there is some high speed flow exiting the diffuser at all heights up to the height of maximum downforce. It can be seen that at all heights up to the maximum downforce a large area between the diffuser surface and the ground is occupied by flow of low turbulence level and high streamwise velocity. This area decreases as the vortices expand in region (b), however at the diffuser ramp there remains a strong flow through the diffuser downstream of the separation bubble. It appears that the separated fluid from the bubble is mostly all pulled into the vortices.

A prominent feature of the flow in the force reduction region (c), is the appearance of asymmetric vortices (Figs. 5(a) and 6(a)). Instead of two broadly symmetric, counter-rotating vortices, the flow in the cross-plane now appears to be dominated by one recognizable vortex. The rest of the flow in the cross-plane is now characterised by a weakly circulating flow and axial flow reversal. The appearance of the main edge vortex appears to be random and was found in the model tests to be influenced by minute changes in model settings. The maximum cross-flow velocities are $|v/U_\infty| = 0.95$ and $|w/U_\infty| = 0.54$ at $h_r/d = 0.204$ (not shown), and 0.57 and 0.49 at $h_r/d = 0.159$ respectively. The peak vorticity, the maximum induced cross-flow velocities are comparable to those in the force plateau region, leading to a high suction level on one side of the diffuser. This observation is supported by the span-wise pressures shown in Fig. 8. However, this suction enhancement mechanism only exists in a small area towards the base of the diffuser (Senior and Zhang, 2001). On the other side, a flow reversal exists which is accompanied by weak cross-flow circulation, the flow reversal being the result of three-dimensional flow separation at the inlet of the diffuser. Once this occurs, a loss of suction is inevitable to one side of the diffuser. Overall the suction loss caused by the flow separation at the diffuser inlet and the apparent break-down of the edge vortex (with the subsequent loss of suction force) now dominate the force production mechanism.

As the model height is further reduced into region (d) (not included), the exit flow is dominated by flow reversal and a rather weak circulating cross-flow. The maximum cross-flow velocities are $|v/U_\infty| = 0.26$ and $|w/U_\infty| = 0.31$ at $h_r/d = 0.064$. The peak vorticity at the centre of the vortex is much lower than those observed at higher model heights ($\Omega d/U_\infty = -0.23$ at $h_r/d = 0.064$). The mass flow entering the diffuser from the inlet is now reduced substantially. Results suggest a generally low diffuser through flow and the presence of large scale flow reversal at both sides of the diffuser. Flow entrainment between the side-plates and the ground is greatly reduced; span-wise velocities under the side-plate are in the order of $w/U_\infty \approx 0.05$. At this height, the gap between the model and the ground is rather small. Measurements at a $h_r/d = 4.14$ suggest that the thickness of the boundary layer underneath the model approaches O(15 mm) before the diffuser inlet. Therefore, the viscous effects should certainly be prominent at this model height. The Reynolds number based on the model height is in the order of 13,000, and for a channel flow, the flow would be fully developed. It is therefore anticipated that the boundary layers underneath the model and over the ground plane have merged at the diffuser inlet at this model height.

The vortices generated in region (b) would have a different effect on any trailing aerodynamic vehicles from those in region (a). Two likely influences are the position of the vortex pair and the strength/size of the vortices. The nature of the counter-rotating vortices and the presence of the ground ensure that the vortices will move away from the ground as they travel downstream. The turbulent vortex cores would lead to a quick dilatation of the vortices. These features will have safety implications.

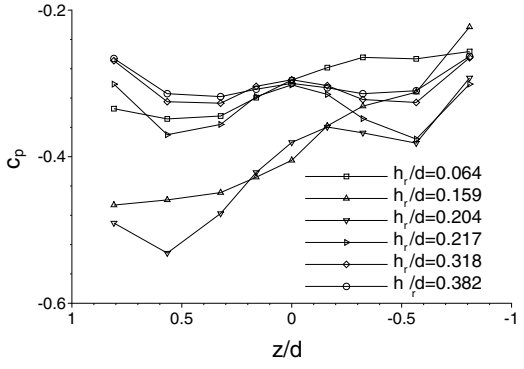

Fig. 8. Spanwise surface pressure distribution near the diffuser exit; $x/d = 7.66$.

4. Summary remarks

A study is conducted of vortex flow behind a bluff body operating in ground effect. The bluff body is equipped with an upswept aft section, generating large downforce and drag on the body. The results reported are obtained under correct ground conditions.

The downforce curve is divided into four distinct regions: force enhancement, force plateau, force reduction, and loss of force. The increase in downforce with model height reduction is attributed to contributions from (a) the upswept surface suction increase, e.g. diffuser effect and (b) edge vortex. A correlation is estab-

lished between the force behaviour and characters of the edge vortex.

In the force enhancement region, the downforce and drag increases with a reduction in model height. The flow is broadly symmetric about the model central plane. A pair of contra-rotating vortices existed in the cross-plane between the upswept surface and the ground. The vortices are generated off the edges of the side plates. The vortices are highly concentrated with a high axial speed core and high vorticity level. The turbulence level at the core is low and the vortices are stable.

In the force plateau region, a 'plateau' in the downforce and drag curves exists over a range of heights towards the upper height limit of the region, which is followed by linear behaviours in the downforce and drag curves. The flow remains broadly symmetric. The sizes of the vortices increases substantially and a low axial speed exists at the core of the vortex. A high level of turbulent stress distribution exists in the vortex. The cause of the initial reduction in slope of the force vs. model height curve is determined to be a reduction in the strength of the vortex.

In the force reduction region, vortex breakdown occurs and a significant portion of downforce is lost. The flow is asymmetric about the model central line. One weakened edge vortex now exists in the cross-plane and a large portion of the area between the diffuser ramp and the ground is occupied by flow reversal, which is attributed to flow separation. Turbulence stress distribution is characterised by high level of mixing between the through flow and the reversal flow.

In the loss of downforce region, the diffuser is starved of mass flow and little activity is observed in the diffuser section.

Acknowledgements

A. Senior and A. Ruhrmann would like to thank the University of Southampton and B.A.R. for financial support. The authors would like to thank W. Toet for discussions.

References

Bearman, P.W., 1980. Review—bluff body flows applicable to vehicle aerodynamics. Journal of Fluids Engineering 102, 265–274.

Benedict, L.H., Gould, R.D., 1996. Towards better uncertainty estimates for turbulence statistics. Experiments in Fluids 22 (2), 129–136.

Brundrett, E., Baines, W., 1964. The production and diffusion of vorticity in duct flow. Journal of Fluids Mechanics 19, 375–394.

Cooper, K.R., Bertenyi, T., Dutil, G., Syms, J., Sovran, G., 1998. The aerodynamic performance of automotive underbody diffusers. SAE Paper 980030.

Cooper, K.R., Sovran, G., Syms, J., 2000. Selecting automotive diffusers to maximise underbody downforce. SAE PAPER 2000-01-0354.

Delery, J.M., 1994. Aspects of vortex breakdown. Progress in Aerospace Science 30, 1–59.

George, A.R., 1981. Aerodynamic effects of shape camber, pitch, and ground proximity on idealized ground vehicle bodies. Journal of Fluids Engineering 103, 631–638.

George, A.R., Donis, J.E., 1983. Flow patterns, pressures, and forces on the underside of idealized ground effect vehicles. ASME, Fluids Engineering Division 7, 69–79.

Jones, R.T., 1990. Wing Theory, first ed. Princeton University Press, Princeton.

Lambourne, N.C., Bryer, D.W., 1962. The bursting of leading-edge vortices—some observations and discussion of the phenomenon. Aeronautical Research Council, R&M No. 3282.

Menke, M., Gursul, I., 1997. Unsteady nature of leading edge vortices. Physics of Fluids 9 (10), 2960–2966.

Moffat, R., 1988. Describing the uncertainties in experimental results. Experimental Thermal and Fluid Science 1, 3–17.

Morel, T., 1978. The effect of base slant on the flow pattern and drag of three-dimensional bodies with blunt ends. In: Aerodynamic Drag Mechanisms of Bluff Bodies and Road Vehicles. Plenum Press, New York, pp. 191–226.

Payne, F.M., Ng, T.T., Nelson, R.C., Schiff, L.B., 1988. Visualisation and wake surveys of vortical flow over a delta wing. AIAA Journal 26 (2), 137–143.

Senior, A.E., Zhang, X., 2001. The force and pressure of a diffuser-equipped bluff body in ground effect. Journal of Fluids Engineering 123, 105–111.

Sovran, G., 1994. The kinematic and fluid-mechanic boundary conditions in underbody flow simulation. In: Proceedings of the CNR-Pininfarina Workshop on Wind Tunnel Simulation of Ground Effect, Turin, Italy, May 1994.

Yeung, A.F.K., Lee, B.H.K., 1999. Particle image velocimetry study of wing-tip vortices. Journal of Aircraft 36 (2), 482–484.

Zhang, X., 1998. Turbulence measurements of a longitudinal vortex generated by an inclined jet in a turbulent boundary layer. ASME Journal of Fluids Engineering 120, 765–771.